Article

Magnetic Properties and Magnetic Structures of Synthetic Natrochalcites, NaM(DO)(MoO), M = Co or Ni

Serge Vilminot, Gilles Andre#, Francoise Boure#e-Vigneron,
Peter J. Baker, Stephen J. Blundell, and Mohamedally Kurmoo

J. Am. Chem. Soc., **2008**, 130 (40), 13490-13499 • DOI: 10.1021/ja804685u • Publication Date (Web): 12 September 2008

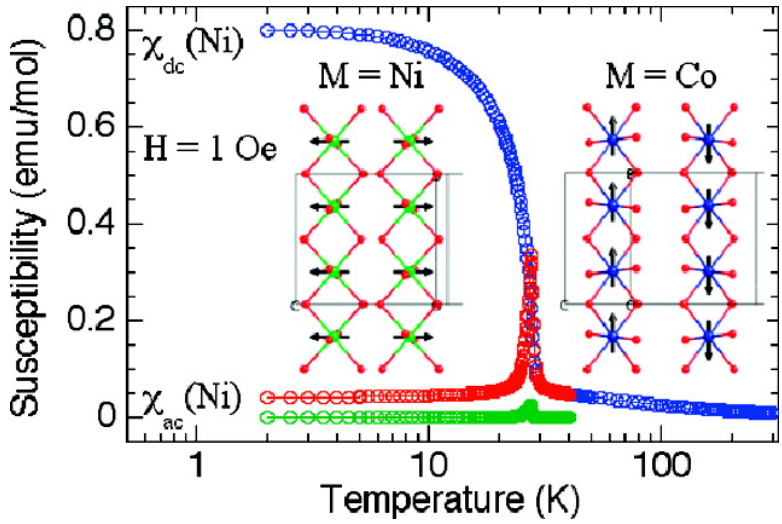

More About This Article

Additional resources and features associated with this article are available within the HTML version:

- Supporting Information
- Access to high resolution figures
- Links to articles and content related to this article
- Copyright permission to reproduce figures and/or text from this article

View the Full Text HTML

J|A|C|S
ARTICLES

Published on Web 09/12/2008

Magnetic Properties and Magnetic Structures of Synthetic Natrochalcites, $NaM^{II}_2(D_3O_2)(MoO_4)_2$, M = Co or Ni

Serge Vilminot,*,† Gilles André,‡ Francoise Bourée-Vigneron,‡ Peter J. Baker,*,§ Stephen J. Blundell,§ and Mohamedally Kurmoo*,||

Groupe des Matériaux Inorganiques, IPCMS, UMR 7504 CNRS-ULP, 23 rue du Loess, BP 43, 67034 Strasbourg Cedex 2, France, Laboratoire Léon Brillouin, CEA-CNRS, CEA-Saclay, 91191 Gif-sur-Yvette Cedex, France, Clarendon Laboratory, University of Oxford, Parks Road, Oxford OX1 3PU, United Kingdom, and Laboratoire de Chimie de Coordination Organique, CNRS-UMR7140, Université Louis Pasteur, Institut Le Bel, 4 rue Blaise Pascal, 67000 Strasbourg Cedex 01, France

Received June 19, 2008; E-mail: vilminot@ipcms.u-strasbg.fr; kurmoo@chimie.u-strasbg.fr; p.baker1@physics.ox.ac.uk

Abstract: The magnetic properties and magnetic structures from neutron diffraction of two synthetic natrochalcites, $NaM^{II}_2(H_3O_2)(MoO_4)_2$, M = Co (**1Co**) or Ni (**2Ni**), are reported. They are isostructural (monoclinic *C*2/*m*) and consist of chains of edge-shared MO_6 octahedra connected by μ-O from $H_3O_2^-$ and MoO_4^{2-}. These chains form a three-dimensional network with O−H−O, O−Mo−O, and O−Na−O bridging 4, 3, and 4 metal ions, respectively. Both compounds behave as canted antiferromagnets but differ in their behaviors, **1Co** showing a broad maximum (28 K) above the Néel transition (21 K) and the canting taking place at 13 K, some 8 K below T_N, while for **2Ni** the canting takes place at T_N (28 K). Analyses of the neutron powder diffraction data shed some light on the geometry of $D_3O_2^-$ and suggest antiferromagnetism with a propagation vector $k = (0,0,0)$ with the moments within each chain being parallel but antiparallel to those in neighboring chains. The difference between **1Co** and **2Ni** is in the orientation of the moments; they are parallel to the chain axis (*b*-axis) for **1Co** and perpendicular to it for **2Ni** with a major component along the *c*-axis and a small one along the *a*-axis. The heat capacity data peak at 20.9(3) K (**1Co**) and 25.1(1) K (**2Ni**). The derived magnetic entropies, following correction of the lattice contribution using the measured data for the nonmagnetic Zn analogue, suggest $S = {}^1/_2$ for **1Co** but is lower than that expected for **2Ni** ($S = 1$). In both cases, only ca. 60% of the entropy is found below the magnetic ordering temperature, suggesting considerable short-range correlations at higher temperatures. While the temperature at which the magnetic diffraction becomes observable coincides with that of at the peak in heat capacity, it is lower than T_N observed by magnetization measurements in both cases, and there is evidence of short-range ordering in a narrow range of temperature ($T_N \pm 5$ K).

Introduction

The magnetism of natural minerals has long been of interest to magneto-chemists, -geologists, and -physicists for their range of structures, colors, textures, and electrical and magnetic properties. Most recently, there has been further development in the field by chemists toward the reproduction of certain minerals in the laboratory using hydrothermal syntheses.[1−3] The latter provide materials of superior qualities with respect to the metal contents, control on the mixture of metals and anions (SO_4 and SeO_4, for example) in alloying, and modification by inclusion of organics.[4−6] These improved and modified materials allow finer studies to be performed. Furthermore, the hydrogen atoms in these structures are generally those of OH and H_2O, which can be easily replaced by deuterium for neutron diffraction studies. Along these lines, we have explored the magnetic properties and magnetic structure determinations from neutron diffraction of several materials having tetrahedral anions such as sulfate and have extended this study to others containing

† IPCMS.
‡ Laboratoire Léon Brillouin.
§ University of Oxford.
|| Université Louis Pasteur.

(1) (a) Harrison, R. J. Magnetic properties of rocks and minerals. *Treatise on Geophysics*; Elsevier: Amsterdam, 2008; Vol. 2, p 579. (b) Schieber, M. M. *Experimental Magnetochemistry*; North-Holland Publishing Co.: Amsterdam, 1967. (c) Goodenough, J. B. *Magnetism and the Chemical Bond*; John Wiley and Sons: New York, 1963.
(2) *Physics Meets Mineralogy*; Aoki, H., Syono, Y., Hemley, R. J., Eds.; CUP: Cambridge, 2000.
(3) (a) Cundy, C. S.; Cox, P. A. *Chem. Rev.* **2003**, *103*, 663, and references therein. (b) Byrappa, K.; Yoshimura, M. *Handbook of Hydrothermal Technology, Technology for Crystal Growth and Material Processing*; William Andrew Publishing: New York, 2001. (c) Barrer, R. M. *Hydrothermal Chemistry of Zeolites*; Academic Press: London, 1982. (d) Rabeneau, A. *Angew. Chem., Int. Ed. Engl.* **1985**, *24*, 1026.
(4) (a) Nocera, D. G.; Bartlett, B. M.; Grohol, D.; Papoutsakis, D.; Shores, M. P. *Chem.-Eur. J.* **2004**, *10*, 3850. (b) Wills, A. S. *Phys. Rev. B* **2001**, *63*, 064430. (c) Shores, M. P.; Nytko, E. A.; Bartlett, B. M.; Nocera, D. G. *J. Am. Chem. Soc.* **2005**, *127*, 13462. (d) Behara, J. N.; Rao, C. N. R. *Can. J. Chem.* **2005**, *83*, 668–673. (e) Behara, J. N.; Rao, C. N. R. *Dalton Trans.* **2007**, 668.
(5) Harrison, A. *J. Phys.: Condens. Matter* **2004**, *16*, S553.
(6) Shores, M. P.; Bartlett, B. M.; Nocera, D. G. *J. Am. Chem. Soc.* **2005**, *127*, 17986.

 10.1021/ja804685u CCC: $40.75

selenate and molybdate.[7−9] In the present study, we examine two natrochalcites, $NaM^{II}_2(H_3O_2)(MoO_4)_2$, where M = Co or Ni.[10]

The mineral natrochalcite, $NaCu_2(OH)(SO_4)_2(H_2O)$, is named after its content Natrium (Na) and Chalcos (Cu) and is naturally found as emerald green crystals grown on acatamite.[10] It is also known for other ZO_4^{2-}, where Z = Se, Mo, Te, or Cr. Giester and Zemann have developed the syntheses of a variety of derivatives where Na has been replaced by K or Rb and S by Se.[11] Twenty years before, Pezerat et al. prepared the corresponding cobalt analogue, $KCo_2(H_3O_2)(MoO_4)_2$,[12] while Palacio et al. reported the crystal structure determined from X-ray powder diffraction data of the sodium compound, $NaCo_2(H_3O_2)(MoO_4)_2$.[13] The latter study was undertaken following a series of reports by Clearfield et al. on the syntheses and structural characterizations of $NaM_2(OH)(H_2O)(MoO_4)_2$, where M = Ni, Mn, and Zn.[14] None of these studies examined the magnetic properties of these compounds. Clearfield et al. also reported related compounds $NaCuOHMoO_4$ and $NaZnOHMoO_4$ belonging to a different structural family.[15] Other known transition metal molybdates are $Ag_2Co_2(MoO_4)_3$, $K_2Ni_2(MoO_4)_3$, $Li_2Co_2(MoO_4)_3$, the mixed-valent cobalt compound $NaCo_{2.31}(MoO_4)_3$ and the monovalent $M^{II}MoO_4$, where M = Cu, Fe, Mn, Co, or Ni.[16,17]

Our interest in the natrochalcite structural types is 2-fold. On the one hand, the existence of chains of edge-shared octahedra with possible Ising-type anisotropy and expected ferromagnetic nearest neighbor interaction, judging from the M−O−M angle of ca. 98°, may result in single-chain magnetic behaviors (slow relaxation), while the presence of an expected weak antiferromagnetic exchange may result in long-range magnetic ordering.[18,19] On the other hand, given that we were to study the magnetic structures at low temperatures by neutron diffraction on deuterated samples, we thought it would be worthwhile to complement the work of Clearfield et al.[14] and Chevrier et al.[20] by performing a statistical analysis of the positions of the hydrogen atoms in H_3O_2 to decide on the exact position of the bridging hydrogen atom. Based on X-ray single crystal diffraction, the centrally placed model has been reported for a series of coordination complexes, *cis*-α-$[\{(pico)_2Cr\}_2(H_3O_2)_2]X_4\cdot 2H_2O$ (X = I or ClO_4), *trans*-$[Cr(py)_2(H_3O_2)_2]Cl$, α-*cis*-$[Cr(bispicen)(H_3O_2)]I_2$, β-*cis*-$[\{Cr(bispictn)\}_2(H_3O_2)]I_4\cdot 4H_2O$, $Na_2[Et_3MeN][Cr(PhC(S)=N(O))_3]\cdot {}^1/_2NaH_3O_2\cdot 18H_2O$, $[LRu^{II}(bqdi)\}_2(\mu\text{-}O_2H_3)](PF_6)_3$, $[\{LRu^{III}(acac)\}_2(\mu\text{-}O_2H_3)](PF_6)_3$ (L = 1,4,7-trimethyl-1,4,7-triazacyclononane and bqdi = *o*-benzoquinone diimine), $\{[M_3O_2(O_2CC_2H_5)_6(H_2O)_2]_2(H_3O_2)\}Br_3\cdot 6H_2O$ (M = Mo or W), and $[Tp'_2Zn_2O_2H_3]ClO_4$ (Tp′ = hydro(3-*p*-isopropylphenyl-5-methylpyrazilyl)borate).[21,22] The chromium compounds have been shown to exhibit weak antiferromagnetic coupling.[21]

Experimental Section

Synthesis. $NaM^{II}_2(H_3O_2)(MoO_4)_2$, where M = Co (**1Co**) or Ni (**2Ni**) or Zn (**3Zn**), was obtained under hydrothermal conditions. For the preparation of **1Co**, cobalt sulfate heptahydrate, $CoSO_4\cdot 7H_2O$ (1.68 g, 6 mmol), and sodium molybdate dihydrate, $Na_2MoO_4\cdot 2H_2O$ (4.35 g, 18 mmol), were separately dissolved in boiling distilled water (35 mL), and the two solutions were quickly mixed while still hot. The resultant violet suspension was immediately poured into the autoclave, which was sealed and heated under autogenous pressure at 240 °C for 24 h. Small violet crystals were obtained. They were thoroughly washed with water, alcohol, and acetone and dried in air at 40 °C. For syntheses at temperatures between 150 and 200 °C, powders are obtained instead of crystals.

(7) (a) Vilminot, S.; Richard-Plouet, M.; André, G.; Swierczynski, D.; Bourée-Vigneron, F.; Marino, E.; Guillot, M. *Cryst. Eng.* **2002**, *5*, 177. (b) Vilminot, S.; Richard-Plouet, M.; André, G.; Swierczynski, D.; Bourée-Vigneron, F.; Kurmoo, M. *Dalton Trans.* **2006**, 1455. (c) Ben Salah, M.; Vilminot, S.; André, G.; Richard-Plouet, M.; Bourée-Vigneron, F.; Mhiri, T.; Kurmoo, M. *Chem.-Eur. J.* **2004**, *10*, 2048. (d) Ben Salah, M.; Vilminot, S.; Mhiri, T.; Kurmoo, M. *Eur. J. Inorg. Chem.* **2004**, 2272. (e) Vilminot, S.; Richard-Plouet, M.; André, G.; Swierczynski, D.; Bourée-Vigneron, F.; Kurmoo, M. *Inorg. Chem.* **2003**, *42*, 6859. (f) Ben Salah, M.; Vilminot, S.; André, G.; Richard-Plouet, M.; Mhiri, T.; Takagi, S.; Kurmoo, M. *Chem. Mater.* **2005**, *17*, 2612. (g) Ben Salah, M.; Vilminot, S.; André, G.; Richard-Plouet, M.; Bourée-Vigneron, F.; Mhiri, T.; Kurmoo, M. *J. Am. Chem. Soc.* **2006**, *128*, 7972.

(8) Vilminot, S.; André, G.; Bourée-Vigneron, F.; Richard-Plouet, M.; Kurmoo, M. *Inorg. Chem.* **2007**, *46*, 10079.

(9) Vilminot, S.; André, G.; Richard-Plouet, M.; Bourée-Vigneron, F.; Kurmoo, M. *Inorg. Chem.* **2006**, *45*, 10938.

(10) http://www.webmineral.com/data/Natrochalcite.shtml.

(11) Giester, G.; Zemann, J. *Z. Kristallogr.* **1987**, *179*, 431.

(12) (a) Pezerat, H. *Bull. Soc. Fr. Mineral. Cristallogr.* **1967**, *90*, 549. (b) Pezerat, H. *C. R. Acad. Sci. Paris* **1965**, *261*, 5490. (c) Pezerat, H.; Mantin, I.; Kovacevic, S. C. R. *Hebd. Séances Acad. Sci., Ser. C* **1966**, *263*, 60. (d) Pezerat, H. C. R. *Hebd. Séances Acad. Sci., Ser. C* **1967**, *265*, 368.

(13) Palacio, L. A.; Echavarra, A.; Saldarriaga, C. *Int. J. Inorg. Mater.* **2001**, *3*, 367.

(14) (a) Moini, A.; Clearfield, A.; Jorgensen, J. D. *Acta Crystallogr.* **1986**, *C42*, 1667. (b) Clearfield, A.; Sims, M. J.; Gopal, R. *Inorg. Chem.* **1976**, *15*, 335. (c) Clearfield, A.; Moini, A.; Rudolf, P. R. *Inorg. Chem.* **1985**, *24*, 4606.

(15) (a) Moini, A.; Peascoe, R.; Rudolf, R. P.; Clearfield, A. *Inorg. Chem.* **1986**, *25*, 3782. (b) Clearfield, A.; Gopal, R.; Saldarriaga-Molina, C. H. *Inorg. Chem.* **1977**, *16*, 628. (c) Marsh, R. E.; Schomaker, V. *Inorg. Chem.* **1979**, *18*, 2331.

(16) (a) Tsyrenova, G. D.; Solodovdikov, S. F.; Khaikina, E. G.; Khobrakova, E. T.; Bazarova, Zh. G.; Solodovdinokova, Z. A. *J. Solid State Chem.* **2004**, *177*, 2158. (b) Klevstsova, R. F.; Glinskaya, L. A. *J. Struct. Chem.* **1982**, *23*, 816.

(17) (a) Ibers, J. A.; Smith, G. W. *Acta Crystallogr.* **1964**, *17*, 190. (b) Ibers, J. A.; Smith, G. W. *Acta Crystallogr.* **1965**, *19*, 269. (c) Ehrenberg, H.; Svoboda, I.; Wltschek, G.; Wiesmann, M.; Trouw, F.; Weitzel, H.; Fuess, H. *J. Magn. Magn. Mater.* **1995**, *150*, 371. (d) Wiesmann, M.; Ehrenberg, H.; Wltschek, G.; Zinn, P.; Weitzel, H.; Fuess, H. *J. Magn. Magn. Mater.* **1995**, *150*, L1. (e) Ehrenberg, H.; Wiesmann, M.; Paulus, H.; Weitzel, H. *J. Magn. Magn. Mater.* **1998**, *186*, 74. (f) Ehrenberg, H.; Schwarz, B.; Weitzel, H. *J. Magn. Magn. Mater.* **2006**, *305*, 57.

(18) (a) Gatteschi, D.; Sessoli, R.; Villain, J. *Molecular Nanomagnets*; Oxford University Press: Oxford, 2006. (b) Blundell, S. J.; Pratt, F. L. *J. Phys.: Condens. Matter* **2004**, *16*, R771. (c) Caneschi, A.; Gatteschi, D.; Lalioti, N.; Sangregorio, C.; Sessoli, R.; Venturi, G.; Vindigni, A.; Rettori, A.; Pini, M. G.; Novak, M. A. *Angew. Chem., Int. Ed.* **2001**, *40*, 1760. (d) Clérac, R.; Miyasaka, H.; Yamashita, M.; Coulon, C. *J. Am. Chem. Soc.* **2002**, *124*, 12837. (e) Coulon, C.; Clérac, R.; Lecren, L.; Wernsdorfer, W.; Miyasaka, H. *Phys. Rev. B* **2004**, *69*, 132408. (f) Coulon, C.; Miyasaka, H.; Clérac, R. *Struct. Bonding (Berlin)* **2006**, *122*, 163. (g) Bogani, L.; Wernsdorfer, W. *Nat. Mater.* **2008**, *7*, 79.

(19) (a) De Jongh, L. J.; Miedema, A. R. *Adv. Phys.* **1974**, *23*, 1. (b) Steiner, M.; Villain, J. *Adv. Phys.* **1976**, *25*, 87.

(20) Chevrier, G.; Giester, G.; Jarosch, D.; Zemann, J. *Acta Crystallogr.* **1990**, *C46*, 175–177.

(21) (a) Ardon, M.; Bino, A.; Michelsen, K. *J. Am. Chem. Soc.* **1987**, *109*, 1990. (b) Ardon, M.; Bino, A.; Michelsen, K.; Petersen, E. *J. Am. Chem. Soc.* **1987**, *109*, 5855. (c) Ardon, M.; Bino, A.; Michelsen, K.; Petersen, E.; Thompson, R. C. *Inorg. Chem.* **1997**, *36*, 4147.

(22) (a) Abu-Dari, K.; Raymond, K. N.; Freyberg, D. P. *J. Am. Chem. Soc.* **1979**, *101*, 3688. (b) Abu-Dari, K.; Freyberg, D. P.; Raymond, K. N. *Inorg. Chem.* **1979**, *18*, 2427. (c) Bino, A.; Gibson, D. *J. Am. Chem. Soc.* **1981**, *103*, 6741. (d) Bino, A.; Gibson, D. *J. Am. Chem. Soc.* **1982**, *104*, 4383. (e) Ruf, M.; Weis, K.; Vahrenkamp, H. *J. Am. Chem. Soc.* **1996**, *118*, 9288. (f) Puerta, D. T.; Cohen, S. M. *Inorg. Chim. Acta* **2002**, *337*, 459. (g) Jüstel, T.; Bendix, J.; Metzler-Nolte, N.; Weyhermüller, T.; Nuber, B.; Wieghardt, K. *Inorg. Chem.* **1998**, *37*, 35. (h) Schneider, R.; Weyhermüller, T.; Wieghardt, K.; Nuber, B. *Inorg. Chem.* **1993**, *32*, 4925.

Moreover, **1Co** is also obtained for different Co:Mo ratios between 1:1 and 1:4. For **2Ni**, a similar synthesis starting from $NiSO_4 \cdot 6H_2O$ resulted in the formation of the related compound. However, broad peaks were evidenced on the X-ray diffraction pattern, which are probably related to some amount of a poorly crystallized phase. This anomaly was not present for the more crystallized **2Ni** samples obtained by replacing nickel sulfate by nickel nitrate, $Ni(NO_3)_2 \cdot 6H_2O$ (1.46 g, 5 mmol), or nickel chloride, $NiCl_2 \cdot 6H_2O$ (1.188 g, 5 mmol), in the presence of $Na_2MoO_4 \cdot 2H_2O$ (3.63 g, 15 mmol), and working under conditions similar to those for **1Co**, that is, 240 °C but for 3 days. Bright green crystals are obtained for a starting Ni:Mo ratio of 1:3. Other ratios resulted in the formation of only powders. $NaZn_2(H_3O_2)(MoO_4)_2$ (**3Zn**) was obtained from zinc sulfate heptahydrate $ZnSO_4 \cdot 7H_2O$ solution (1.438 g, 5 mmol, in 20 mL of H_2O) and sodium molybdate dihydrate $Na_2MoO_4 \cdot 2H_2O$ solution (3.629 g, 15 mmol, in 20 mL of H_2O) at 220 °C for 2 days. A white powder is obtained, and it was washed with water, alcohol, and acetone.

Deuterium-rich samples (**1CoD** and **2NiD**) for neutron diffraction measurements were synthesized under the same conditions starting from $CoSO_4 \cdot 7H_2O$ or $Ni(NO_3)_2 \cdot 6H_2O$, $Na_2MoO_4 \cdot 2H_2O$, and D_2O. The use of D_2O is to reduce the incoherent scattering from hydrogen that would give rise to an increase of the background and a poor signal-to-background ratio that can complicate further analysis.

Physical Measurements Techniques. Thermal analyses were performed in air at a 5 °C/min heating rate by use of a TA-STD-Q600 apparatus. The samples were placed in a Pt crucible. Infrared spectra were recorded using a Digilab Excalibur Series FTIR spectrometer by transmission through KBr pellets containing 1% of the crystals. EDX analyses for the heavy metals were made using a Kevex unit of a JEOL 6700 F. Powder X-ray diffraction patterns were recorded using a D500 Siemens diffractometer (Co $K\alpha_1$, 1.789 Å) for the cobalt samples and a D5000 Siemens diffractometer (Cu $K\alpha_1$, 1.5406 Å) for nickel and zinc samples; both diffractometers are equipped with a front monochromator. Magnetic susceptibility measurements were performed in the temperature range 2−300 K and field range ±50 kOe using a Quantum Design MPMS-XL SQUID magnetometer at Strasbourg and field range ±70 kOe of a MPMS-XL SQUID magnetometer at Oxford. Ac susceptibility measurements were performed using the same equipment. Heat capacity measurements were carried out on pressed pellets of the three compounds using a Quantum Design Physical Property Measurement System at Oxford. This employs a standard relaxation time technique, and the data are corrected by removal of a previously determined background due to the sample mount and Apiezon grease.

Single crystal X-ray diffraction data for **1Co** were collected at 173 K on a Nonius Kappa CCD diffractometer using monochromated Mo $K\alpha_1$ radiation. The structure was solved by means of a three-dimensional Patterson function and refined using SHELXS-97 and SHELXL-97 programs.[23] The final refinement included anisotropic displacement parameters and a secondary extinction correction. Difference Fourier maps did not reveal the position of the hydrogen atoms. Additional experimental details are given in Table 1. Table 2 gives the final atomic positions, and Table 3 gives the corresponding bond lengths and angles. Further details of the crystal-structure investigation may be obtained from the CIF file, which has been deposited at the Fachinformationzentrum Karlsruhe, 76344 Eggenstein-Leopoldshafen, Germany, on quoting the depository number CSD-418002 (they can be requested from Crysdata @FIZ-Karlsruhe.de).

The neutron diffraction experiments were performed at the Laboratoire Léon Brillouin (CEA Saclay) using the 3T2 and G4.1 diffractometers. Data obtained on the high-resolution powder diffractometer 3T2 (λ = 1.22525 Å, 6.85° < 2θ < 121.9°) were used for the refinement of the nuclear structure at 300 K and those from the 800 cells multidetector G4.1 (λ = 2.4266 Å) diffractometer for the determination of the magnetic structures and their thermal evolutions. Eighteen diffraction patterns were recorded in the 2θ range 12°−91.9°, at different temperatures between 1.5 and 30 K for **1CoD** and 11 diffraction patterns in the 2θ range 9°−89° at temperatures between 1.4 and 31 K for **2NiD**. The powder samples were set in cylindrical vanadium containers and held in a liquid helium cryostat. Nuclear and magnetic structures were refined using the FULLPROF program.[24] The nuclear scattering lengths (b_{Co} = 0.249 × 10^{-12} cm, b_{Ni} = 1.03 × 10^{-12} cm, b_{Mo} = 0.6715 × 10^{-12} cm, b_{Na} = 0.363 × 10^{-12} cm, b_O = 0.5803 × 10^{-12} cm, b_D = 0.6671 × 10^{-12} cm, and b_H = −0.3739 × 10^{-12} cm) and cobalt and nickel magnetic form factors were those included in this program.

Table 1. Summary of the Single-Crystal X-ray Data for **1Co** Taken at 173 K

a (Å)	9.3557(9)	μ (mm^{-1})	7.117
b (Å)	6.3269(6)	hkl range	$-12 < h < 13$ $-8 < k < 8$ $-9 < l < 5$
c (Å)	7.6248(7)	θ range (deg)	4.03−30.01
β (deg)	115.784(2)	total number of reflections	1111
V (Å^3)	406.40(7)	unique reflections	514
Z	2	unique $\lvert I_o\rvert > 2\sigma(I_o)$	444
space group	$C2/m$ (12)	R_{int} (%)	0.020
F (000)	462	R_F (all data) (%)	0.0365
D_{calcd} (g cm^{-3})	4.043	wR2(F_o^2) (all data) (%)	0.093
radiation λ (Å)	Mo $K\alpha_1$ 0.71073	GOF (%)	1.207

Table 2. Fractional Atomic Coordinates for **1Co** Obtained from X-ray Data at 173 K

atom	x/a	y/b	z/c	U_{iso} (Å^2)
Mo	0.08047(7)	0	0.28676(11)	0.0048(3)
Co	0.25	0.25	0	0.0056(3)
Na	0	0.5	0.5	0.0103(11)
OH	0.3516(6)	0	0.9143(10)	0.0064(13)
O1	0.7656(7)	0	0.4825(10)	0.0129(15)
O2	0.4618(5)	0.7273(6)	0.2586(8)	0.0081(10)
O3	0.8312(6)	0	0.8829(9)	0.0081(14)

Table 3. Bond Distances (Å) and Angles (deg) for **1Co** from the X-ray Structure Refinement at 173 K

	Co Environment		
Co−OH	2.091(4) × 2	OH−Co−OH	180.0(3)
Co−O2	2.106(5) × 2	OH−Co−O2	88.5(2) × 2
Co−O3	2.113(4) × 2	OH−Co−O2	91.5(2) × 2
⟨Co−O⟩	2.103	OH−Co−O3	82.1(2) × 2
		OH−Co−O3	97.9(2) × 2
		O2−Co−O2	180.0
		O2−Co−O3	91.2(2) × 2
		O2−Co−O3	88.8(2) × 2
		O3−Co−O3	180.0
	Mo Environment		
Mo−O1	1.722(7)	O1−Mo−O2	109.0(2) × 2
Mo−O2	1.772(4) × 2	O1−Mo−O3	106.9(3)
Mo−O3	1.813(6)	O2−Mo−O2	108.5(3)
⟨Mo−O⟩	1.770	O2−Mo−O3	111.7(2) × 2
	Na Environment		
Na−O1	2.546(6) × 2	O1−Na−O1	180.0
Na−O2	2.433(5) × 4	O1−Na−O2	77.63(14) × 4
⟨Na−O⟩	2.471	O1−Na−O2	102.37(14) × 4
		O2−Na−O2	89.7(2) × 2
		O2−Na−O2	180.0 × 2
		O2−Na−O2	90.3(2) × 2

Results and Discussion

Synthesis. Several synthetic approaches to the natrochalcite family of compounds have been reported in the literature,[11−15]

(23) Sheldrick, G. M. *Acta Crystallogr.* **2008**, *A64*, 112.

comprising refluxing aqueous solutions of metal(II) chloride and sodium molybdate for nickel (Ni:Mo = 1:4) and zinc (Zn:Mo = 1:1) and hydrothermal at 200 °C for 3 days for cobalt (Co:Mo = 1:1). For manganese, a combination of reflux and hydrothermal was used. We have obtained the three compounds under study here by the hydrothermal synthesis. From our results, it appears that an excess of sodium molybdate favors the formation of crystals, a ratio M:Mo = 1:3 being the most favorable. The formation of a basic molybdate is explained by the pH value of the sodium molybdate solution. EDX analyses for **1Co** and **2Ni** confirm the Na:M:Mo of 1:2:2.

X-ray Powder Diffraction. From the X-ray powder diffraction data for **1Co** and **2Ni** compounds, their structures have been refined starting from the unit cell parameters and atomic positions obtained from the structure analysis using a single crystal of **1Co** or those given by Palacio et al. from Rietveld refinement.[13] Good fits were obtained with space group *C*2/*m* and lattice parameters for **1Co** of $a = 9.3925(7)$ Å, $b = 6.3319(5)$ Å, $c = 7.6252(6)$ Å, $\beta = 115.876(4)°$, $V = 408.0(1)$ Å^3 and for **2Ni** of $a = 9.3355(9)$ Å, $b = 6.2540(5)$ Å, $c = 7.5900(6)$ Å, $\beta = 115.887(4)°$, $V = 398.7(1)$ Å^3. The lack of additional peaks and the good agreements between calculated and observed diffraction profiles confirm the formation of only **1Co** and **2Ni**, exhibiting the natrochalcite-type structure. Using the pattern matching routine, the unit cell parameters of **3Zn** were determined to be $a = 9.430(2)$, $b = 6.337(1)$, $c = 7.642(1)$ Å, $\beta = 115.804(7)°$, which are in agreement with those in the JCPDS file no. 70-161. The neutron diffraction data, in addition, allowed us to confirm the presence of $D_3O_2^-$ and to determine its geometry in this series.

Thermal Properties. The three compounds exhibit similar DT-TGA behaviors in air except for the temperatures of the transformations (see text and Figures S1−S3 of ESI). The compounds first lose the H_3O_2 group endothermically as H_2O. For **1Co**, two weight gains are observed followed by a weight loss associated with oxidation−reduction ($CoO-Co_3O_4$). Two sharp endotherms correspond to the formation of $NaCo_{2.3}(MoO_4)_3$ (JCPDS file no. 72-1066) and $CoMoO_4$ (JCPDS file no. 25-1434).[17] In argon (Figure S1), the oxidation of CoO is absent. For **2Ni**, the weight increase is continuous from 615 to 900 °C (Figure S2). An annealed sample at 900 °C for 1 h reveals the formation of α-NiMoO4 (JCPDS file no. 31-902) and $Na_{1.9}Ni_{1.05}(MoO_4)_2$ (JCPDS file no. 77-798).

The most striking observation in the DT-TGA experiments is the variation of the temperature for the departure of H_3O_2 as a function of the metal. It suggests that the associated M−O bond strength is in the order Zn < Co < Ni. The order for the last two cations appears to be generally observed in other coordination polymers.

Infrared Spectroscopy. The infrared spectra of the three compounds are fairly similar with slight differences in peak positions (Table S1, Figures S4−S6). Consequently, we discuss those of the cobalt compounds, $NaCo_2(H_3O_2)(MoO_4)_2$ (**1Co**) and $NaCo_2(D_3O_2)(MoO_4)_2$ (**1CoD**), which reveal the presence of the OH or OD and MoO_4 vibration bands and differentiate between them. The first ones are shifted when D substitutes H. In both cases, the O−H(D) valence stretching modes at 3343 and 3110 (2496 and 2321) cm^{-1} appear as very broad bands. This is related to the presence of strong hydrogen (deuterium) bonds as previously mentioned. When the OH groups are involved in weak hydrogen bonds, one observes a rather sharp band, for instance, in the case of lindgrenite.[9] Moreover, the bending mode of $H(D)_2O$, usually observed around 1600(1200) cm^{-1}, is very weak in the case of **1Co** and **1CoD**. Four bands are related to the vibrations of the molybdate group, 928(933) cm^{-1} attributed to ν_1 that becomes IR active due to the deformation of the tetrahedron, 860(862), 827(832), and 771(784) cm^{-1} attributed to ν_3.[25] For **1CoD**, two new bands appear at 658 and 568 cm^{-1} that have been attributed to libration modes. The corresponding O−H bands are therefore expected in the same regions as those of MoO_4^{2-} and hidden by these bands. Below 500 cm^{-1}, other bands at 403(403), 354(363), 336(333), 293(297), 237(241) cm^{-1} are present and are at nearly the same positions for **1Co** and **1CoD**. They could be related either to Co−OH(D) vibrations or to ν_2 and ν_4 of molybdate.

The H_3O_2 has nine normal coordinates involving the five atoms. The OH stretching modes are expected to be similar to those of water molecule. However, the bending mode may be severely constrained due to the connection to another OH, which may be the reason for the weak intensity. Additional symmetric, antisymmetric stretching and bending modes are expected for the O−H−O central part. In the case of HF_2^- ion,[25] which is also linear, two modes are IR active, at 1233 (ν_2) and 1450 cm^{-1} (ν_3). For **1Co**, the two bands at 1168 cm^{-1} and the shoulder at 910 cm^{-1} strongly decrease for **1CoD** and have been attributed to the vibrations of the O−H−O central part. For **2Ni** and **3Zn**, the first band is shifted to 1185 and 1139 cm^{-1}, respectively, probably in relation to the variation of the mass of the M element bonded to O. For the other band, it is difficult to distinguish between ν_1 (MoO_4) and ν (O−H−O).

Crystal Structures. Although the nuclear structures of these compounds have been reported using both powder and single-crystal diffraction data for their determinations,[13,14,20] in the present study we confirm these structures and furthermore realized a more accurate determination of the structure of the cobalt compound from single-crystal diffraction data (Tables 1−3). In addition, the neutron powder diffraction data at low temperatures provided evidence that the structures remain unaltered as well as the geometry of $D_3O_2^-$ (Tables S2−S7).[14,20] Consequently, we will keep our description of the structure short and highlight the pertinent information needed for the discussion of the magnetic properties and magnetic structures that will follow.

$NaM_2(H_3O_2)(MoO_4)_2$ forms an isostructural set having the natrochalcite structure, which consists of chains of edge-shared MO_6 octahedra running along the *b*-axis and where the metals are located at $^1/_4a$ and $^3/_4a$ (Figure 1).[13,14,20] The M−M distance of less than 3.2 Å and M−O−M angles of ∼98° provide the primary magnetic exchange pathway, and these values are expected to result in ferromagnetic interaction between nearest moment carriers.[26] The cobalt and nickel ions are in almost a regular octahedral environment with M−O distances slightly shorter for nickel, ⟨Ni−O⟩ = 2.092 Å, ⟨Co−O⟩ = 2.103 Å (X-rays) and 2.107 Å (neutrons), as expected due to its smaller ionic radius, 0.74 Å as compared to 0.80 Å for Co^{2+} (Tables 3, S4, and S7). These chains are then connected by three kinds of three-atom bridges involving H_3O_2, MoO_4, and NaO_6 (Figure

(24) Rodriguez-Carvajal, J. *FULLPROF: Rietveld, profile matching and integrated intensity refinement of X-ray and/or neutron data, 3.5d version*; Léon-Brillouin Laboratory/CEA Saclay: France, 2005.

(25) Nakamoto, K. *Infrared and Raman Spectra of Inorganic and Coordination Compounds*, 4th ed.; John Wiley & Sons: New York, 1986.

(26) (a) Weihe, H.; Güdel, H. U. *J. Am. Chem. Soc.* **1998**, *120*, 2870. (b) Hay, P. J.; Thibeault, J. C.; Hoffmann, R. *J. Am. Chem. Soc.* **1975**, *97*, 4884.

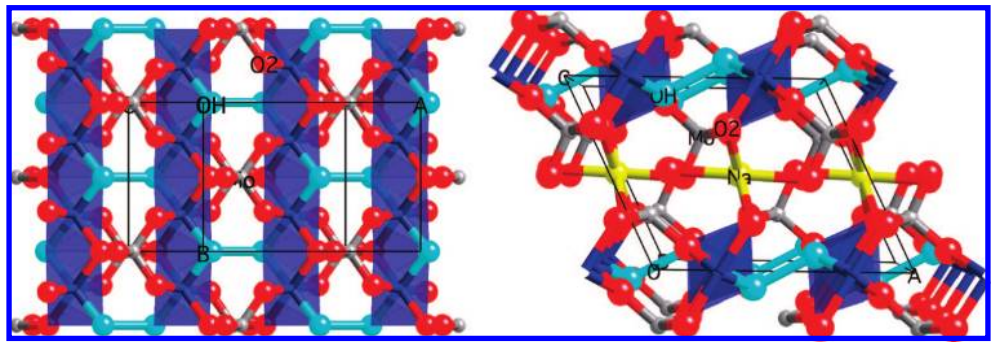

Figure 1. Views of the structure of **1Co** along the chain axis (*b*-axis, left) and of an *ab*-layer (right) showing the connections of the chains by the MoO_4 and H_3O_2: cobalt (blue), molybdenum (gray), oxygen (red (MoO_4) and cyan (H_3O_2)), sodium (yellow).

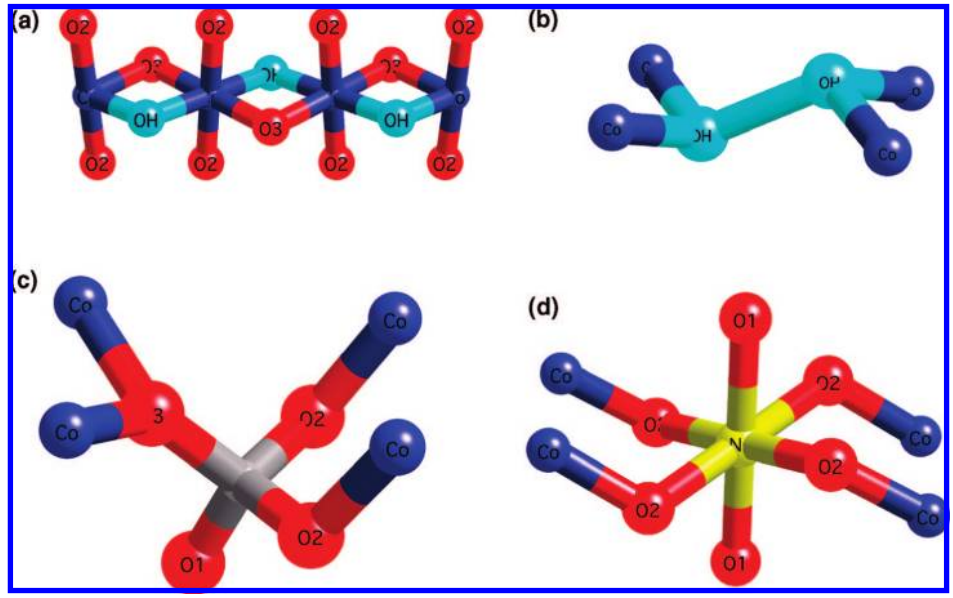

Figure 2. Views of the connections for **1Co** between the metal centers (a) along a chain and through (b) H_3O_2, (c) MoO_4, and (d) NaO_6.

Table 4. Summary of the Refinements Concerned with the Position of the D2 Atom

model	D2 position	OD···OD (Å)	OD−D2 (Å)	OD−D1 (Å)	R_p, R_{wp}, R_B, R_F (%)
A	0.5, 0, 0	2.545(5)	1.272(4) × 2	0.982(6)	12.0, 12.8, 5.79, 3.90
B	0.5, *y*, 0	2.546(5)	1.284(10) × 2	0.984(6)	12.5, 13.4, 6.61, 4.16
	y = 0.0259 (118)				
C	*x*, 0.5, *z*	2.544(5)	1.102(14)	0.981(6)	11.8, 12.7, 5.50, 3.70
	x = 0.0202(15)	2.487(1)[a]	1.096(3)[a]		
	0.01876(38)[a]		1.449(13)	0.980(1)[a]	
	z = 0.0244(17)		1.392(3)[a]		
	0.01207(114)[a]				

[a] Values from Chevrier et al..[20]

2). The first two connect the chains in the *a*-axis direction to form layers along *ab*, while Na connects these layers in a 3D network through the oxygen atoms of the MoO_4 units. All three connections provide secondary magnetic pathways between four magnetic centers of adjacent ferromagnetic chains. The MoO_4 are slightly irregular, as observed by both X-rays and neutron diffraction, with Mo−O distances between 1.695 and 1.865 Å, that is, a distortion of nearly 10%, (1.865−1.695)/⟨Mo−O⟩, for **2Ni**, while it is 5.1% (X-rays), 6.6% (neutrons at 296 K) for **1Co**. The sodium ions are in a distorted octahedral environment, with very similar Na−O distances for both compounds.

All the oxygen atoms are of μ_3-type but with different atomic environments: OH(D) is bonded to M, H(D)1, and H(D)2, O1 to Mo, Na, and H(D)1 through a hydrogen (deuterium) bond, O2 to Mo, Co, and Na, and O3 to Mo and M (twice) (Tables 3 and S3). Concerning the hydrogen (deuterium) bonding, the discussion will be focused on the results obtained from the high-resolution 3T2 diffractometer data recorded at 300 K. The refinements have been done using three possible models: (A) D2 is placed on the center of symmetry, (B) D2 is allowed to occupy two positions equally along the *b*-axis direction, and (C) D2 is allowed to occupy two positions equally in the *ac*-plane. Table 4 summarizes the results for **1CoD**. It also allows a direct comparison with the results obtained from neutron diffraction data on a single crystal of $KCu_2(H_3O_2)(SO_4)_2$ at 300 K.[20]

For **1Co**, the three models converge to similar R_p, R_{wp}, R_B, and R_F values except for model B, where the R_B and R_F values

Table 5. Results of Bond Valence (*s*) Calculations around OH(D) Atoms

atom[a]	*s* H_2O	*s* OH^-	*s* $H_3O_2^-$
H1	0.767	0.767	0.767
H2	0.561	0.252	0.376
Cu	0.440 × 2	0.440 × 2	0.440 × 2
$\sum s$	2.208	1.899	2.023
atom[b]	*s* D_2O	*s* OD^-	*s* $D_3O_2^-$
D1	0.864	0.864	0.862
D2	0.623	0.244	0.394
Co	0.342 × 2	0.342 × 2	0.341 × 2
$\sum s$	2.171	1.792	1.938

[a] For $KCu_2(H_3O_2)(SO_4)_2$. [b] For $NaCo_2(D_3O_2)(MoO_4)_2$.

are higher. Therefore, it is difficult to conclude on a particular model. Chevrier et al. concluded that H2 position is split (model C),[20] resulting in the presence of H_2O and OH^- groups and the superposition with the symmetry related pair. In contrast, the centrally placed H2 model (A) yields the existence of $H_3O_2^-$ ion with a symmetrical O−H−O. This debate may be resolved by calculating the bond energies, which is not the goal of this Article. Symmetrical hydrogen bonding is rarely observed, the most well-known being the HF_2^- ion, where H is located at the midpoint between F atoms with F···F = 2.27 Å. As compared to the sum of the corresponding van der Waals radii, 3.00 Å, this means that hydrogen bonding in HF_2^- promotes a bond shortening of 0.73 Å and explains the value of ΔH for dissociation of 1 mol bonds of 155 kJ.[27] In hydrofluoric acid (HF), the hydrogen bond is unsymmetrical, and both the bond shortening, 0.51 Å, and ΔH, 29 kJ, are correspondingly decreased. For hydrogen bonding involving oxygen atoms, the bond shortening is smaller than in the case of the more electronegative F^- ion. In ice, the bond shortening and ΔH values are 0.24 Å and 21 kJ, respectively. For H(D)2, the OH(D)···OH(D) distances are 2.487(1) Å (Cu) and 2.545(5) Å (**1CoD** at room temperature) corresponding to a bond shortening of 0.55 and 0.50 Å as compared to the sum of the van der Waals radii, 3.04 Å. These values are of the same order as the one observed for the HF_2^- ion, 0.67 Å. Bond valence calculations are reported in Table 5 for both compounds.[28]

From Table 5, it appears that the sum of the bond valence values around the OH(D) atoms is much closer to the expected value of 2 for model A. The presence of strong D bonds can therefore explain the high thermal stability of the compounds with weight losses starting at 420 °C (**2Ni**) and 335 °C (**1Co**). In conclusion, some arguments are in favor of the existence of the $H_3O_2^-$ ion with a symmetrical O−H−O bridge.

Magnetic Properties. The temperature dependence of the magnetic susceptibilities of the two magnetic compounds is quite different (Figure 3). For **1Co**, the susceptibility is field independent from 300 to about 25 K where there is a maximum. Above 150 K, the inverse susceptibility follows the Curie−Weiss law with a Curie constant of 7.64(1) emu K/mol and a Weiss constant of −47(1) K. The calculated effective moment of 5.53 μ_B per cobalt is slightly higher than that expected, and the negative Weiss constant means dominant antiferromagnetic exchange.[29] At 25 K, the susceptibility shows a maximum, indicating other weaker antiferromagnetic interactions come into play. Considerable field dependence is observed below 13 K, which also coincides with a peak in the ac-susceptibility and the bifurcation in the ZFC-FC magnetization in a small field and thus marks a point of spontaneous magnetization. The strong field dependence suggests it may be a canted antiferromagnetic material. This is confirmed by the nonsaturation and linear dependence of the isothermal magnetization with field up to 50 kOe at 2 K (Figure 4a). Using the remanant magnetization of 0.007 μ_B per cobalt and assuming a saturation value of 2.4 μ_B per cobalt, the estimated canting angle for a two-sublattice system $[\sin^{-1}(0.007/2.4)]$ is 0.17(1)°.

The temperature dependence of the magnetic susceptibility of **2Ni** is much simpler (Figure 3b). The high temperature susceptibility, being independent of field, fits the Curie−Weiss equation with a Curie constant of 2.784(3) emu K/mol per two nickel and a Weiss constant of −12.9(3) K. At 28 K, spontaneous magnetization is observed, which is very sensitive to the applied field and is accompanied by a sharp peak in both the real and the imaginary ac-susceptibilities. The isothermal magnetization at 2 K is almost linear with field without reaching saturation and shows a small hysteresis loop with a coercive field of ca. 1 kOe and a remanant magnetization of 0.012 μ_B per nickel (Figure 4b). The temperature and field dependence of the magnetization are characteristics of a canted antiferromagnet. Using the same approach as for **1Co** and the expected 2 μ_B per Ni^{2+}, we estimate a canting of 0.30(1)°. In contrast to **1Co**, the canting takes place at the Néel temperature for **2Ni** and not below it.

Specific Heat Measurements. The pseudoadiabatic heat capacities for the three isostructural compounds were measured from 2 to 200 K using a relaxation technique.[30] Data were taken in two independent runs for each compound and merged after corrections for the contributions of the sample holder and grease using the data from a previously measured blank under the same experimental conditions. The temperature dependence of the molar heat capacities normalized by the temperature is presented in Figure 5. They are dominated by the lattice contribution, and for the magnetic compounds λ-like anomalies are observed at the corresponding long-range magnetic ordering temperature.

Given the reliability of the data over such a wide range of temperature measured, we proceed by fitting the heat capacity data for **3Zn** using a function with two Einstein modes and a Debye mode, allowing the characteristic temperatures (θ_i) and amplitudes (A_i) of each component to vary. The best fit is shown in Figure 5. The values obtained are presented in Table 6. We find that the total amplitude of the lattice modes is somewhat less than the Dulong−Petit value we would expect the fit to approach at high temperature. This is likely to be due to higher energy modes that do not affect the data significantly in our measured temperature range. To determine the lattice contribution for the magnetic Co and Ni compounds, the same function was fitted to the heat capacity data for temperatures above 40 K, fixing the amplitudes of the three components to the values found for the Zn complex and allowing the characteristic temperatures to vary independently. The amplitudes are given in Table 6.

(27) Porterfield, W. W. *Inorganic Chemistry: A Unified Approach*, 2nd ed.; Academic Press: San Diego, CA, 1993; p 200.
(28) Brown, I. D.; Altermatt, D. *Acta Crystallogr.* **1985**, *B41*, 244.
(29) (a) Mulay, L. N., Boudreaux, E., Eds. *Theory of Molecular Paramagnetism*; Wiley: New York, 1976. (b) Morrish, A. H. *The Physical Principles of Magnetism*; R. E. Krieger: Huntington, NY, 1980.
(30) Lashley, J. C.; et al. *Cryogenics*2003, *43*, 369.

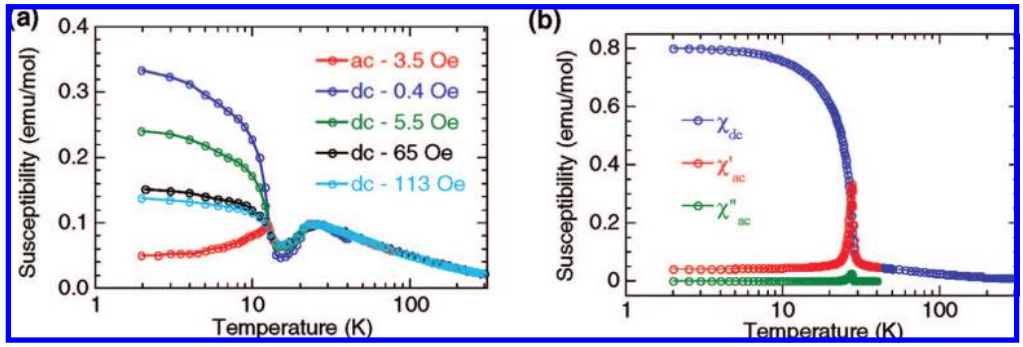

Figure 3. Magnetic susceptibilities (ac and dc) measured at different applied field for **1Co** (a) and for **2Ni** (b).

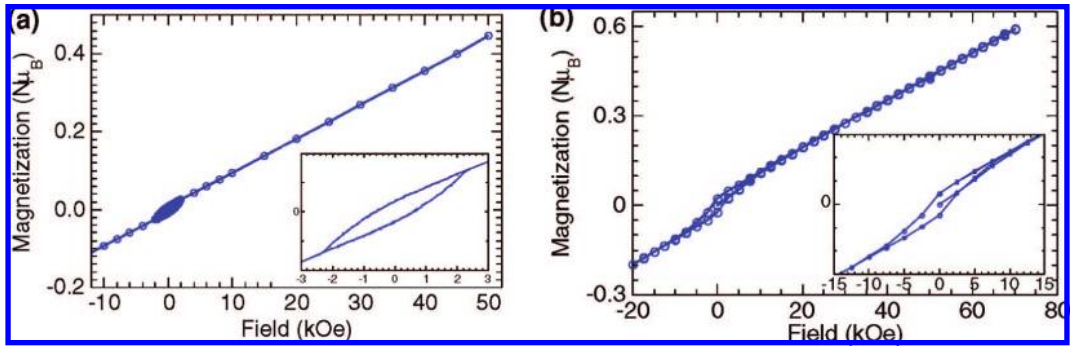

Figure 4. Isothermal magnetization at 2 K for **1Co** (a) and **2Ni** (b).

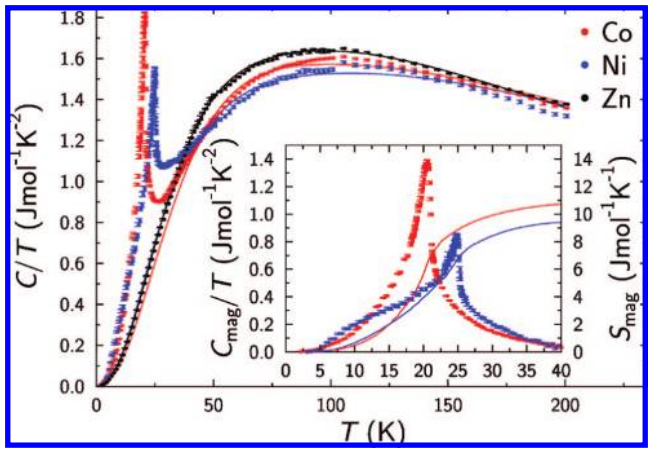

Figure 5. Heat capacities *C*/*T* of the three compounds with lines showing the fitted lattice contribution described in the text. Inset: Magnetic contributions to the heat capacity for **1Co** and **2Ni** with the integrated magnetic entropy shown with the solid lines.

Table 6. Parameters Determined from Fitting the Function Described in the Text to the Heat Capacity Data from the Three Compounds[a]

compd	A_D (J mol^{-1} K^{-1})	A_{E1} (J mol^{-1} K^{-1})	A_{E2} (J mol^{-1} K^{-1})	θ_D (K)	θ_{E1} (K)	θ_{E2} (K)
3Zn	80(5)	175(4)	102(4)	169(4)	510(15)	230(8)
1Co				186(2)	619(4)	260(2)
2Ni				173(2)	621(5)	283(3)

[a] The A_D, A_{E1}, and A_{E2} values found for the **3Zn** complex were fixed in the analysis for **1Co** and **2Ni**.

The magnetic contributions to the heat capacity for **1Co** and **2Ni** were determined by subtracting the functions described above from the measured data, using the parameters listed in Table 6. These are shown in the inset of Figure 5, together with the magnetic entropy sums shown with the solid lines. The total magnetic entropy values were 10.8 J mol^{-1} K^{-1} for **1Co** and 9.5 J mol^{-1} K^{-1} for **2Ni**. The magnetic ordering temperatures of 20.9(3) K (**1Co**) and 25.1(1) K (**2Ni**) were obtained. Only around 60% of the magnetic entropy is released below the long-range ordering (LRO) temperature in each case, suggesting that a major part is due to short-range correlations. Furthermore, for **2Ni** a broad hump centered at 12 K may be due to a Schottky anomaly derived from single-ion anisotropy of the $S = 1$ Ni^{2+}.[31]

Magnetic Structures. The powder neutron diffraction patterns of **1CoD** and **2NiD** at 30 K, that is, above the magnetic transitions, match well with those calculated, but slightly contracted unit cell, using the nuclear lattice parameters from the 3T2 results as a starting model. At temperatures below T_N, several additional Bragg reflections of magnetic origin are observed (Figure 6). For every temperature, all of the reflections can be indexed within the same unit cell; thus the propagation vector is $k = (0,0,0)$. The additional reflections in the patterns at low temperature (1.5 K) as compared to those at 29.7 K (**1CoD**) or 31.1 K (**2NiD**) clearly highlight that the magnetic structures of the two compounds are different (Figure 7). For instance, the (101) line being the second strongest magnetic Bragg reflection for **1CoD** is absent for **2NiD** (see, for example, the difference diffraction patterns in Figures S7 and S8). For **1CoD**, the magnetic lines correspond to diffraction planes $(\pm h,0,l)$ with h odd that are forbidden for the $C2/m$ space group. For **2NiD**, (h,k,l) planes are additionally observed. When the temperature of the samples is increased from the lowest one, in addition to these new sharp reflections a hump starts to develop at 14.8 K for **1CoD** and 18.2 K for **2NiD** (Figure S9). It reaches a maximum at 18.6 K (**1CoD**) and 25.1 K (**2NiD**), and then decreases, nearly disappearing at 29.7 K (**1CoD**) or still present

(31) Blundell, S. J.; Blundell, K. M. *Concepts in Thermal Physics*; Oxford University Press: Oxford, 2006.

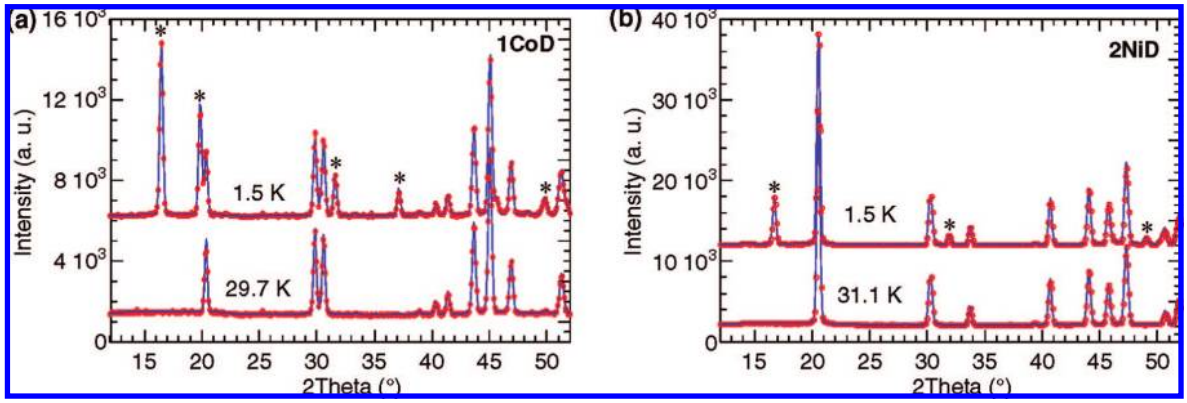

Figure 6. Part of the observed neutron diffraction patterns (red ○) above and below the magnetic transitions and the Rietveld refinements (lines) for **1CoD** (a) and **2NiD** (b). The asterisks mark some of the magnetic reflections below the Néel transitions.

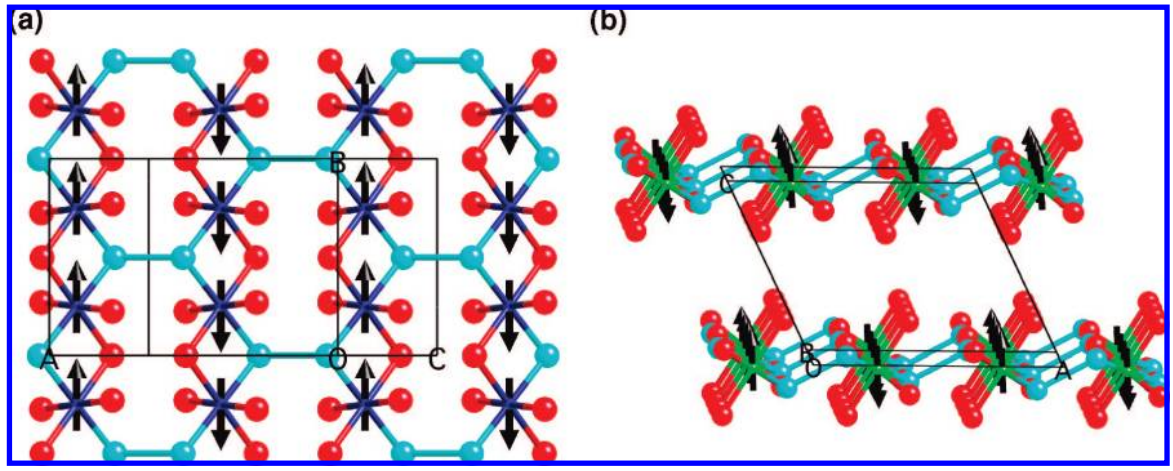

Figure 7. Orientation of the moments in the LRO magnetic structures of **1Co** (a) and **2Ni** (b).

Table 7. Basis Functions of the Irreducible Representations, Γ_2 and Γ_4[a]

IR	moment	M11	M12	M13	**M14**
Γ_2	M_x, M_y, M_z	+ + +	− + −	− − −	+ − +
Γ_4	M_x, M_y, M_z	+ + +	+ − +	− − −	− + −

[a] M11 ($^1/_4$, $^1/_4$, 0); M12 ($^3/_4$, $^1/_4$, 0); M13 ($^3/_4$, $^3/_4$, 0); M14 ($^1/_4$, $^3/_4$, 0).

at 31.1 K (**2NiD**). However, it must be noticed that the relative increase of the background is more visible for **1CoD** (up to 26%) as compared to **2NiD** (up to 9%).

To help find solutions to the magnetic structures from the data recorded at the lowest temperature, we determined the associated magnetic structures using Bertaut's representation analysis method,[32] applied to the *C*2/*m* space group, $k = (0,0,0)$ propagation vector and M in 4e Wyckoff position. Two one-dimensional irreducible Γ_2 and Γ_4 representations are associated with basis vectors (magnetic structures) for M (Table 7).[33] As expected from the observed difference between the low temperature data, different models, Γ_2 for **2NiD** and Γ_4 for **1CoD**, were found to reach agreement between observed and calculated patterns (Figures S10 and S11).

For **1CoD**, refinements allowing three-dimensional freedom of all of the moments resulted in insignificant values of M_z, and thus it was set to zero. Two possibilities have consequently been checked, one with the moments along the *b*-axis and the other with moments within the *ab*-plane. The latter model resulted in a very low value of M_x of 0.385(130) μ_B, just less than $3\sigma(M_x)$. Therefore, the final adopted model is that where all of the moments are parallel to the chain (*b*-axis). However, while they are all parallel within one chain of the unit cell, those in the neighboring chain are antiparallel to them, giving an overall compensated antiferromagnet (Table S8, Figure 7). The uncertainties in the derived moments do not allow us to resolve the small canting angles suggested by the magnetic measurements. The calculated magnetic moment per cobalt, summing over all of the sharp magnetic Bragg reflections from the long-range ordering (2.95(2) μ_B), is found to be close to the expected 3 μ_B per cobalt. It is constant from 1.5 to 10 K, and it slowly decreases to reach zero at 18.6 K (Figure 8). In contrast, that of the short-range ordering is zero up to 14 K, and it increases slowly and tends toward saturation about 25 K. There is an overlap of both LRO and SRO between 14 and 17.7 K. Assuming that the volume distribution of both phases, long-range order LRO and short-range order SRO, is homogeneous, we have refined the latter using the same model as for the former but with an adjustable coherence length. The SRO coherent length is at a maximum of 25 Å at 14 K. For the highest recorded temperature, 29.7 K, the SRO signals have nearly disappeared. It is also worth noting that the LRO sets in below

(32) Bertaut, F. *Acta Crystallogr.* **1968**, *A24*, 217.
(33) (a) Hovestreydt, E.; Aroyo, I.; Sattler, S.; Wondratschek, H. *J. Appl. Crystallogr.* **1992**, *25*, 544; KAREP: A program for calculating irreductible space group representations. (b) Rodriguez-Carvajal, J. *BASIREPS: A program for calculating non-normalized basis functions of the irreductible representations of the little group Gk for atom properties in a crystal*; Laboratoire Léon Brillouin (CEA-CNRS): CEA Saclay: Gif-sur-Yvette, France, 2004.

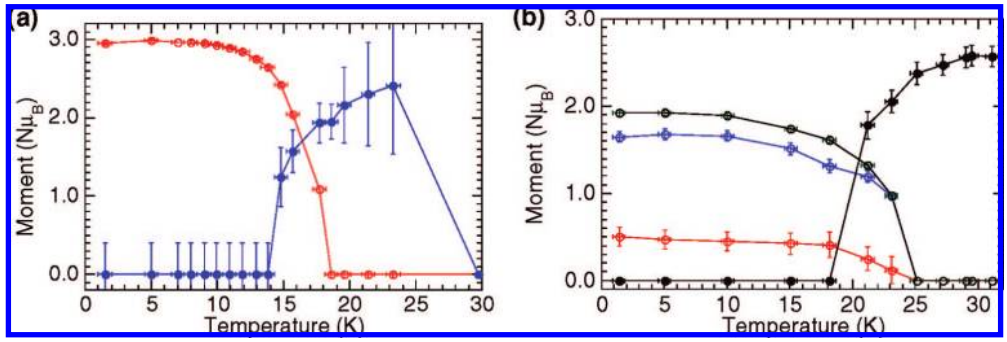

Figure 8. Temperature dependence of the magnetic moments for (a) **1CoD** (LRO, red ○ and SRO, blue ●) and (b) **2NiD** (LRO, M_x, red ○; M_z, blue ○; M_{total}, ○; and SRO, ●).

18.6 K, while the heat capacity peaks at 21 K and the estimated Néel temperature from the magnetization measurements is around 23 K. This anomaly may be an indication that the magnetic length is shorter than the diffraction length, and thus the magnetization is more sensitive to the ordering within smaller size clusters thus observable at a higher transition temperature.

Proceeding in a similar way for the refinement of the magnetic structure of **2NiD** (Figure 7), it is clearly observed that the M_y component is not significant, and it has therefore been set to zero. Further refinements performed with the magnetic moment vectors either along the *c*-axis or within the *ac*-plane suggest that the second model is better, with a R_{mag} factor of 8.4 instead of 12.0%. The final result is that the moments are aligned along *c**, that is, a magnetic vector of 1.7 μ_B along the *c*-axis and 0.5 μ_B along the *a*-axis (Table S9, Figure 7). The derived total magnetic moment per nickel (1.92(3) μ_B) is nearly the expected 2 μ_B at the lowest temperature. While the *a*-axis component is almost independent of temperature until it reaches zero at 25 K, that of the *c*-axis has a pronounced temperature dependence, also reaching zero at 25 K (Figure 8). Again, we find the transition temperature for the magnetic ordering to be different, being at 28 K in magnetization measurements and below 25.1 K from neutron scattering.

An overlay of the diffraction patterns for **2Ni** at different temperatures indicates that a broad background is also present as for **1CoD** in the same angular region, which is therefore attributed to SRO. The SRO component has also been refined using the same procedure as for **1CoD**. However, due to the low intensity, the analyses overestimate the magnetic moment (2.0 μ_B expected for Ni^{2+}).

According to these results, the magnetic structures (Figure 7) of $NaM_2(D_3O_2)(MoO_4)_2$ with M = Ni or Co consist of ferromagnetically aligned moments within a chain of M ions, and the moments of the second chain within the unit cell are antiparallel to the first one, resulting in an antiferromagnetic structure as expected from the susceptibility measurements. While the magnetic moments are aligned in the direction of the chain axis for **1CoD**, they are perpendicular to the chain axis for **2NiD**.

The results of the neutron diffraction suggest that the single-atom bridge within each chain provides ferromagnetic exchange between nearest neighbors, while the three-atom bridges, O−H−O, O−Mo−O, and O−Na−O, generate antiferromagnetic exchange. One anomaly is that the Weiss temperature is negative for both compounds. This may be the case if the absolute exchange interaction is larger for the antiferromagnetic ones than for the ferromagnetic one. Given that the angle of 98° for M−O−M is borderline between AF and F, the M−O−M exchange energy may be small.[26] The difference in the transition temperatures found by magnetization measurements as compared to those from neutron diffraction and heat capacity remains to be understood. One possible mechanism may involve the way the coherent length of the magnetic correlation varies as a function temperature parallel and perpendicular to the chain axis. We expect the length scale to be longer perpendicular to the chain than parallel to it if the transverse exchange is larger. Thus the shape of the volume of correlated moments will look like a flattened disk just below the transition, and the ratio of the long to short axis will decrease as the temperature of the samples is lowered to become more spherical. This contrasts with the expected rod-like shape of the correlated Ising spins in a single-chain magnet in which the correlation length is longer in the chain direction than perpendicular to it. If some transverse interactions come into play, long-range magnetic ordering may take place at lower temperature where a ferromagnetic ground state is expected for transverse ferromagnetic exchange or an antiferromagnetic ground state for antiferromagnetic exchange.[34] For the latter, below T_N a metamagnetic critical field may be observed at which the moments can be reversed to the ferromagnetic state. However, if the chains are ferrimagnetic, a ferrimagnet will be the ground state in zero-field for positive transverse exchange or in high-field for negative exchange.[35] A slight difference in the propagation of the sphere as a function of temperature may also be responsible for the difference in behavior of the temperature dependence magnetic susceptibility between the two compounds.[36] The magneto-crystalline anisotropy is also important, and, in our opinion, it accounts for the canting at a lower temperature for **1Co**.[37]

Conclusion

Using a wide range of techniques, correlation of the nuclear and magnetic structures to the magnetic properties of two natrochalcites, $NaM^{II}_2(H_3O_2)(MoO_4)_2$, M = Co or Ni, is provided. Most importantly, the difference in anisotropy of the two metal ions results in different orientations of the moments, and it also contributes to the contrasting temperature dependence

(34) Kurmoo, M.; Kumagai, H.; Chapman, K. W.; Kepert, C. J. *Chem. Commun.* **2005**, 3012.
(35) Kurmoo, M.; Kumagai, H.; Akita-Tanaka, M.; Inoue, K. *Inorg. Chem.* **2006**, *45*, 1627.
(36) De Jongh, L. J., Ed. *Magnetic Properties of Layered Transition Metal Compounds*; Kluwer Academic Publishers: Dordrecht/Boston, MA, 1990.
(37) (a) Dzyaloshinski, I. *J. Phys. Chem. Solids* **1958**, *4*, 241. (b) Moriya, T. *Phys. Rev.* **1960**, *120*, 91.

of the magnetic susceptibilities. The fact that the long-range magnetic ordering temperatures, measured from magnetization, are a few degrees higher than those where magnetic reflections start to appear or where the heat capacity peaks has been associated with the different length scales. We have presented arguments detailing why we observed long-range magnetic ordering and not single-chain magnetism as well as under what conditions metamagnetism can be observed for chain compounds. We believe a similar study of the analogous manganese and iron compounds may help in confirming our hypothesis, as the former will be isotropic and the latter more anisotropic than the cobalt and nickel analogues.

Acknowledgment. We acknowledge the CNRS (France) and EPSRC (U.K.) for financial support. This work is dedicated to Prof. Peter Day on the occasion of his 70th birthday.

Supporting Information Available: Tables of infrared bands and assignments, nuclear structure details from neutron diffraction, and derived magnetic moments as a function of temperature. Full ref 30 and description of DT-TGA, figures of DT-TGA, infrared spectra, and neutron diffraction patterns.This material is available free of charge via the Internet at http://pubs.acs.org.

JA804685U